Fully Multidimensional Flux-Corrected Transport Algorithms for Fluids

Steven T. Zalesak

Naval Research Laboratory, Washington, D.C. 20375

The theory of flux-corrected transport (FCT) developed by Boris and Book [*J. Comput. Phys. 11* (1973) 38; *18* (1975) 248; *20* (1976) 397] is placed in a simple, generalized format, and a new algorithm for implementing the critical flux limiting stage in multidimensions without resort to time splitting is presented. The new flux limiting algorithm allows the use of FCT techniques in multidimensional fluid problems for which time splitting would produce unacceptable numerical results, such as those involving incompressible or nearly incompressible flow fields. The "clipping" problem associated with the original one dimensional flux limiter is also eliminated or alleviated. Test results and applications to a two dimensional fluid plasma problem are presented.

I. Introduction: FCT Defined

Consider the following system of equations

$$w_t + f_x = 0 \tag{1}$$

where w and f are vector functions of independent variables x and t. A simple example of such a system of equations would be the one dimensional equations of ideal, inviscid fluid flow:

$$w = \begin{pmatrix} \rho \\ \rho v \\ \rho E \end{pmatrix}; \qquad f = \begin{pmatrix} \rho v \\ \rho v^2 + P \\ \rho v E + P v \end{pmatrix}$$

where ρ, v, P and E are the fluid density, velocity, pressure and specific total energy respectively.

We shall say that a finite difference approximation to Eq. (1) is in conservation (or "flux") form when it can be written in the form

$$w_i^{n+1} = w_i^{\,n} - \Delta x_i^{-1}[F_{i+(1/2)} - F_{i-(1/2)}] \tag{2}$$

Here w and f are defined at the spatial grid points x_i and temporal grid points t^n, and $\Delta x_i \equiv \frac{1}{2}(x_{i+1} - x_{i-1})$. The $F_{i+(1/2)}$ are called transportive fluxes, and are functions of f at one or more of the time levels t^n. The functional dependence of F on f *defines*

335

the integration scheme (leapfrog, Lax–Wendroff, Crank Nicholson, donor cell, etc.)

It is well known that higher order (order 2 and above) schemes for numerically integrating Eq. (1) suffer from dispersive "ripples" in w, particularly near steep gradients in w. Lower order schemes, such as donor cell, Lax-Friedrichs, or high order schemes with a zeroth order diffusion added, produce no ripples but suffer from excessive numerical diffusion. Flux-corrected transport (FCT) is a technique developed by Boris and Book [1–3] which embodies the best of both of the above worlds. In its simplest terms, FCT constructs the net transportive flux point by point (*non* linearly) as a weighted average of a flux computed by a low order scheme and a flux computed by a high order scheme. The weighting is done in a manner which insures that the high order flux is used to the greatest extent possible without introducing ripples (overshoots and undershoots). This weighting procedure is referred to as "flux-correction" or "flux-limiting" for reasons which shall become clear later. The result is a family of transport algorithms capable of resolving moving contact discontinuities over 3–4 grid points, and shock fronts over 2 grid points, *without* undershoot or overshoot [1–3]. Formally, the procedure is as follows:

(1)   Compute $F^L_{i+(1/2)}$, the transportive flux given by some low order scheme guaranteed to give monotonic (ripple-free) results for the problem at hand

(2)   Compute $F^H_{i+(1/2)}$, the transportive flux given by some high order scheme

(3)   *Define* the "antidiffusive flux":

$$A_{i+(1/2)} \equiv F^H_{i+(1/2)} - F^L_{i+(1/2)}$$

(4)   Compute the updated low order ("transported and diffused") solution:

$$w_i^{td} = w_i{}^n - \Delta x_i^{-1}[F^L_{i+(1/2)} - F^L_{i-(1/2)}]$$

(5)   *Limit* the $A_{i+(1/2)}$ in a manner such that w^{n+1} as computed in step 6 below is free of extrema not found in w^{td} or w^n:

$$A^C_{i+(1/2)} = C_{i+(1/2)}A_{i+(1/2)}, \qquad 0 \leqslant C_{i+(1/2)} \leqslant 1$$

(6)   Apply the limited antidiffusive fluxes:

$$w_i^{n+1} = w_i^{td} - \Delta x_i^{-1}[A^C_{i+(1/2)} - A^C_{i-(1/2)}]$$

The critical step in the above is, of course, step 5 which will be discussed shortly. In the absence of the flux limiting step ($A^C_{i+(1/2)} = A_{i+(1/2)}$), w^{n+1} would simply be the time-advanced high order solution.

We note that this definition of FCT is considerably more general than has been given previously. In this new format, the range of FCT's applicability is seen to be quite large, extending to any fluid transport scheme for which the difference between a low order monotonic time advancement operator and a higher order operator can be written as an array of fluxes between adjacent grid points. This could include both

implicit and explicit Eulerian schemes as well as finite element and Lagrangian methods. For Lagrangian schemes in particular, it is possible that the resolution of shock waves could be improved dramatically by defining "antidiffusive fluxes" that are equal and opposite to the fluxes due to artificial viscosity. For multidimensional Lagrangian codes, this last application was an impossibility before the development of the new flux limiting algorithm to be described in Sections IV and VI.

We also note that the hybridization techniques of Harten and Zwas [8] can be placed in the above format by performing some algebraic manipulation and replacing step 5 by an algorithm completely different from those to be described here. Thus the differences between hybridization and FCT are due entirely to the differences in the all-important step 5.

II. Multidimensional Flux-Corrected Transport

Before proceeding to a discussion of flux limiting, let us see how the procedure given above might be implemented in multidimensions. An obvious choice would be to use a Strang-type time-splitting procedure [4] when it can be shown that the equations allow such a technique to be used without serious error. Indeed, such a procedure may even be preferable from programming and time-step considerations. However, there are many problems for which time-splitting produces unacceptable numerical results, among which are those involving incompressible or nearly incompressible flow fields. This technique is straightforward and shall not be discussed here. Instead we consider as an example the fully two-dimensional set of equations

$$w_t + f_x + g_y = 0 \tag{3}$$

where w, f, and g are vector functions of x, y, and t. In finite difference flux form we have

$$w_{i,j}^{n+1} = w_{i,j}^n - \Delta V_{i,j}^{-1}[F_{i+(1/2),j} - F_{i-(1/2),j} + G_{i,j+(1/2)} - G_{i,j-(1/2)}] \tag{4}$$

where now w, f and g are defined on spatial grid points x_i, y_j at time levels t^n, and $\Delta V_{i,j}$ is a two dimensional area element centered on grid point (i, j). Now there are two sets of transportive fluxes F and G, and the FCT algorithm proceeds as before:

(1) Compute $F_{i+(1/2),j}^L$ and $G_{i,j+(1/2)}^L$ by a low order monotonic scheme
(2) Compute $F_{i+(1/2),j}^H$ and $G_{i,j+(1/2)}^H$ by a high order scheme
(3) *Define* the antidiffusive fluxes:

$$A_{i+(1/2),j} \equiv F_{i+(1/2),j}^H - F_{i+(1/2),j}^L$$

$$A_{i,j+(1/2)} \equiv G_{i,j+(1/2)}^H - G_{i,j+(1/2)}^L$$

(4) Compute the low order time advanced solution:

$$w_{i,j}^{td} = w_{i,j}^n - \Delta V_{i,j}^{-1}[F_{i+(1/2),j}^L - F_{i-(1/2),j}^L + G_{i,j+(1/2)}^L - G_{i,j-(1/2)}^L]$$

(5) Limit the antidiffusive fluxes

$$A_{i+(1/2),j}^C = A_{i+(1/2),j}C_{i+(1/2),j} \qquad 0 \leqslant C_{i+(1/2),j} \leqslant 1$$

$$A_{i,j+(1/2)}^C = A_{i,j+(1/2)}C_{i,j+(1/2)} \qquad 0 \leqslant C_{i,j+(1/2)} \leqslant 1$$

(6) Apply the limited antidiffusive fluxes:

$$w_{i,j}^{n+1} = w_{i,j}^{td} - \Delta V_{i,j}^{-1}[A_{i+(1/2),j}^C - A_{i-(1/2),j}^C + A_{i,j+(1/2)}^C - A_{i,j-(1/2)}^C]$$

As can be easily seen, implementation of FCT in multidimensions is straightforward with the exception of Step 5, an algorithm for which is the subject of this paper. First, however, let us see how flux limiting is presently implemented in one spatial dimension.

III. Flux Limiting in One Spatial Dimension—The Original Algorithm

The original algorithm for flux-limiting in one dimension was given by Boris and Book [1]. In our notation it is:

$$A_{i+(1/2)}^C = S_{i+(1/2)} \max\{0, \min[|A_{i+(1/2)}|,$$

$$S_{i+(1/2)}(w_{i+2}^{td} - w_{i+1}^{td})\,\Delta x_{i+1}, S_{i+(1/2)}(w_i^{td} - w_{i-1}^{td})\,\Delta x_i]\} \qquad (5)$$

where

$$S_{i+(1/2)} = \begin{cases} +1 & \text{if} \quad A_{i+(1/2)} \geqslant 0 \\ -1 & \text{if} \quad A_{i+(1/2)} < 0 \end{cases}$$

The intent of this formula is that antidiffusive fluxes should neither create new extrema, nor accentuate already existing extrema, in the transported and diffused solution w^{td}. That the above formula does, in fact, perform precisely this task can be verified by the reader with relative ease. We shall examine here some of the less obvious properties of this formula. In the process we shall gain insight into which of these properties we shall wish to carry over into a multidimensional flux limiter. We first observe that certain quantities do *not* appear in the above formula: (1) $w_{i+1}^{td} - w_i^{td}$, the first difference of w^{td} at the point where the antidiffusive flux $A_{i+(1/2)}$ is evaluated; and (2) antidiffusive fluxes other than $A_{i+(1/2)}$. This last property is the most notable since there are conceivably two fluxes directed into or out of a cell. A formula guaranteeing that the two fluxes *acting in concert* shall not create ripples would apparently require a knowledge of *both*. We shall return to this point momentarily.

In Fig. 1 we show the eight possible configurations of w^{td} in the neighborhood of a positive $A_{i+(1/2)}$ (directed to the right in our diagrams). Configurations 1–4 show the "normal" situation, with $A_{i+(1/2)}$ having the same sign as $w_{i+1}^{td} - w_i^{td}$ (as might be

expected of an "antidiffusive flux"). We note that if *either* $w_{i+2}^{td} - w_{i+1}^{td}$ or $w_i^{td} - w_{i-1}^{td}$ has a sign opposed to that of $A_{i+(1/2)}$, as in configurations 2–4, the antidiffusive flux $A_{i+(1/2)}$ is *completely canceled* (that is, $A_{i+(1/2)}^C = 0$). This, however, is in total agreement with the stated intent of Eq. (5) since otherwise configuration 2 would allow accentuation of an existing maximum, configuration 3 accentuation of an existing minimum, and configuration 4 accentuation of both. In the remaining
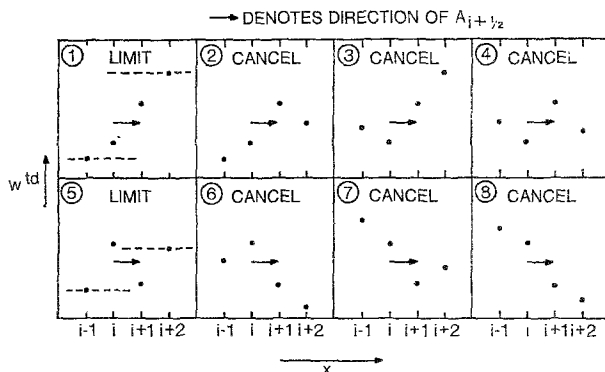
FIG. 1. The eight possible configurations of the transported and diffused solution w^{td} in the neighborhood of a positive (rightward-directed) antidiffusive flux $A_{i+(1/2)}$. Note that configurations 1 through 4 differ from configurations 5 through 8 only in the sign of the quantity $(w_{i+1}^{td} - w_i^{td})$.

configuration 1, the flux limiter (5) will reduce the magnitude of $A_{i+(1/2)}$ sufficiently to guarantee that neither a maximum at grid point $i + 1$ nor a minimum at grid point i will be formed, again in precise agreement with its stated intent.

Configurations 5–8 are identical to configurations 1–4, respectively, except that sign of $w_{i+1}^{td} - w_i^{td}$ has been reversed (The "antidiffusive fluxes" are now directed *down* the gradient in w^{td}). Since the sign of $w_{i+1}^{td} - w_i^{td}$ does not enter into the flux correction formula (5), the results of the formula are identical to those for the previous four cases: the antidiffusive fluxes are canceled for configurations 6–8 and limited in configuration 5 to the extent necessary to prevent a new maximum at grid point $i + 1$ and a new minimum at grid point i. Examination of configurations 6–8 reveals that $A_{i+(1/2)}$ actually presented no hazard insofar as extrema creation or enhancement (at least in moderation). Certainly there was no cause for completely canceling the flux. Even in configuration 5 the flux may have been limited to a greater extent than necessary. At first it would seem that configurations 5–8 represent errors introduced by the simplicity of the flux limiting formula (5). However, extensive tests by this author indicate that in the relatively rare instances in which configurations 5–8 occur in practice, the "errors" introduced by Eq. (5) represent, in fact, the correct action to take in terms of producing accurate profiles in w^{n+1}. More importantly, they represent the mechanism by which Eq. (5) can guarantee that ripples are not formed under any circumstances, as we shall see presently.

Consider two antidiffusive fluxes, acting in concert, attempting to produce or

accentuate an extremum. We therefore have $A_{i+(1/2)}$ and $A_{i-(1/2)}$ either both directed toward, or both directed away from grid point i. We see from Fig. 1 that, in general, an antidiffusive flux directed opposite to the gradient in w^{td} will be completely canceled. Therefore the only cases of fluxes acting in concert that we need be concerned with are those where two adjacent fluxes are both parallel to the local gradients in w^{td}. These are precisely the cases of already existing extrema, in which case *both* fluxes will be canceled (as in configurations 2–4). This is the reason that Eq. (5) needs no information on any antidiffusive flux other than $A_{i+(1/2)}$.

In Fig. 2 we see that the above-mentioned assumptions regarding antidiffusive fluxes acting in concert break down completely in multidimensions. It *is* possible in more than one dimension for more than one antidiffusive flux to be directed into or
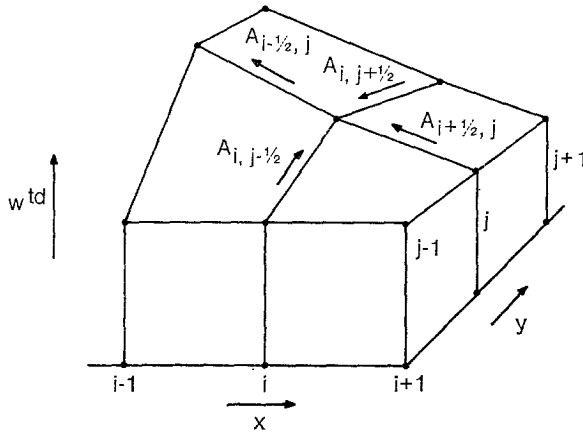

FIG. 2. Perspective view of a two dimensional profile of the transported and diffused solution w^{td}, showing the four possible antidiffusive fluxes affecting the grid point (i, j), the directions of which are indicated by arrows. Note that all of the fluxes are parallel to the local gradient in w^{td} (as "antidiffusive" fluxes might be expected to be), and that $w^{td}_{i,j}$ is not an extremum. This situation is impossible in one dimension, and it is precisely this impossibility which allows fluxes to be limited without regard to neighboring fluxes (see text). In two or more spatial dimensions a flux-limiting formula *must* take into account effects due to multiple fluxes acting in concert.

out of a cell, all of these fluxes being directed parallel to the local gradient in w^{td}, without that cell being an already existing extremum. Therefore the problem of dealing with multiple antidiffusive fluxes acting in concert cannot be avoided by simply canceling all fluxes antiparallel to the local gradient in w^{td}. It is clear then that any formula which purports to perform flux limiting in more than one dimension without resort to time splitting *must* contain information about antidiffusive fluxes other than the one being limited.

IV. FLUX LIMITING IN ONE SPATIAL DIMENSION—AN ALTERNATIVE ALGORITHM

We describe here in one spatial dimension an alternative flux limiting algorithm which generalizes easily to multidimensions and which, even in one dimension, exhibits

a superiority to the limiter described in the previous section (Eq. (5)) with regard to peaked profiles.

Referring to Fig. 3, we seek to limit the antidiffusive flux $A_{i+(1/2)}$ such that

$$A^C_{i+(1/2)} = C_{i+(1/2)} A_{i+(1/2)} , \qquad 0 \leqslant C_{i+(1/2)} \leqslant 1 \tag{6}$$

and such that $A^C_{i+(1/2)}$ acting in concert with $A^C_{i-(1/2)}$ will not allow

$$w^{n+1}_i = w^{td}_i - \Delta x^{-1}_i [A^C_{i+(1/2)} - A^C_{i-(1/2)}]$$

to exceed some maximum value w^{max}_i nor fall below some minimum value w^{min}_i. We leave the determination of w^{max}_i and w^{min}_i until later.

We define three quantities:

$$P^+_i = \text{the sum of all antidiffusive fluxes } into \text{ grid point } i$$
$$= \max(0, A_{i-(1/2)}) - \min(0, A_{i+(1/2)}) \tag{7}$$

$$Q^+_i = (w^{max}_i - w^{td}_i) \Delta x_i \tag{8}$$

$$R^+_i = \begin{cases} \min(1, Q^+_i/P^+_i) & \text{if} \quad P^+_i > 0 \\ 0 & \text{if} \quad P^+_i = 0 \end{cases} \tag{9}$$
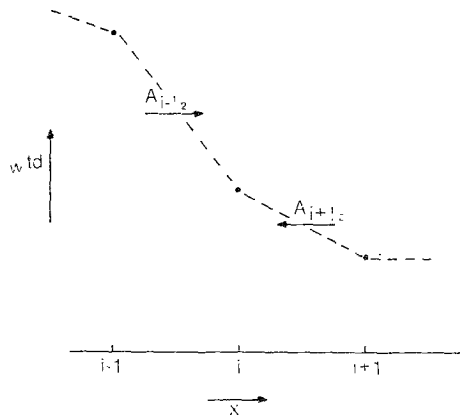

FIG. 3. One dimensional view of the transported and diffused profile w^{td}, showing the two anti-diffusive fluxes $A_{i+(1/2)}$ and $A_{i-(1/2)}$ whose collective effect must be taken into account with respect to overshoots and undershoots in the final value of w^{n+1}_i.

Assuming that $w^{max}_i \geqslant w^{td}_i$ (it must be), all three of the above quantities are positive and R^+_i represents the least upper bound on the fraction which must multiply all antidiffusive fluxes $into$ grid point i to guarantee no overshoot at grid point i.

Similarly we define three corresponding quantities:

$$P^-_i = \text{the sum of all antidiffusive fluxes } away \text{ } from \text{ grid point } i$$
$$= \max(0, A_{i+(1/2)}) - \min(0, A_{i-(1/2)}) \tag{10}$$

$$Q_i^- = (w_i^{td} - w_i^{min}) \Delta x_i \tag{11}$$

$$R_i^- = \begin{cases} \min(1, Q_i^-/P_i^-) & \text{if } P_i^- > 0 \\ 0 & \text{if } P_i^- = 0 \end{cases} \tag{12}$$

Again assuming that $w_i^{min} \leqslant w_i^{td}$, we find that R_i^- represents the least upper bound on the fraction which must multiply all antidiffusive fluxes *away from* grid point i to guarantee no undershoot at grid point i.

Finally we observe that all antidiffusive fluxes are directed away from one grid point and into an adjacent one. Limiting will therefore take place with respect to undershoots for the former and with respect to overshoots for the latter. A guarantee that neither event comes to pass demands our taking a minimum:

$$C_{i+(1/2)} = \begin{cases} \min(R_{i+1}^+, R_i^-) & \text{if } A_{i+(1/2)} \geqslant 0 \\ \min(R_i^+, R_{i+1}^-) & \text{if } A_{i+(1/2)} < 0 \end{cases} \tag{13}$$

Furthermore, we shall call upon our previously described experience with the original flux limiter and set

$$A_{i+(1/2)} = 0 \quad \text{if } A_{i+(1/2)}(w_{i+1}^{td} - w_i^{td}) < 0$$

$$\text{and either} \quad A_{i+(1/2)}(w_{i+2}^{td} - w_{i+1}^{td}) < 0$$

$$\text{or} \quad A_{i+(1/2)}(w_i^{td} - w_{i-1}^{td}) < 0 \tag{14}$$

In practice the effect of Eq. (14) is minimal and is primarily cosmetic in nature. This is because cases of antidiffusive fluxes directed down gradients in w^{td} are rare, and even when they occur usually involve flux magnitudes that are small compared to adjacent fluxes. If Eq. (14) is used, it should be applied *before* Eq. (6) through (13).

We come now to a determination of the quantities w_i^{max} and w_i^{min} in Eqs. (8) and (11). A safe choice is

$$w_i^{max} = \max(w_{i-1}^{td}, w_i^{td}, w_{i+1}^{td}) \tag{15}$$

$$w_i^{min} = \min(w_{i-1}^{td}, w_i^{td}, w_{i+1}^{td}) \tag{16}$$

This choice will produce results identical with those of Eq. (5) in one dimension, including the occurrence of the "clipping" phenomenon to be mentioned shortly.

A better choice is:

$$w_i^a = \max(w_i^n, w_i^{td})$$
$$w_i^{max} = \max(w_{i-1}^a, w_i^a, w_{i+1}^a) \tag{17}$$

$$w_i^b = \min(w_i^n, w_i^{td})$$
$$w_i^{min} = \min(w_{i-1}^b, w_i^b, w_{i+1}^b) \tag{18}$$

This choice allows us to look back to the previous time step for upper and lower bounds on w_i^{n+1}.

It is clear that these two methods of determining w_i^{max} and w_i^{min} represent only a small subset of possible methods. The alternative flux limiter described in Eqs. (6)

through (14) admits of any physically motivated upper and lower bound on w_i^{n+1} supplied by the user, introducing a flexibility unavailable with the original flux limiter (5). However, with the exception of one example in the next section (which shows graphically the potential power of this flexibility), we shall henceforth use Eq. (17) and (18) to evaluate w^{max} and w^{min} in one dimension.

V. COMPUTATIONAL EXAMPLES—ONE DIMENSION

We consider one dimensional passive convection in a constant velocity field. We have Eq. (1) with $w = \rho$ and $f = \rho v$ with $v =$ constant. We choose our transport algorithm to be that given in [3] for LPE Shasta. On the standard square wave tests we find that our results for the original flux limiter (5) and for the alternative flux limiter (6) through (14) are identical to within round-off (the same is true for traveling shock waves in the coupled one dimensional equations of ideal inviscid fluid flow). To find differences between the limiters in one dimension we must look to passive convection of peaked profiles. We choose the problem given by Forester [5], a gaussian of half-width $2 \Delta x$. In Fig. 4 we show the results after 600 iterations for the trivial
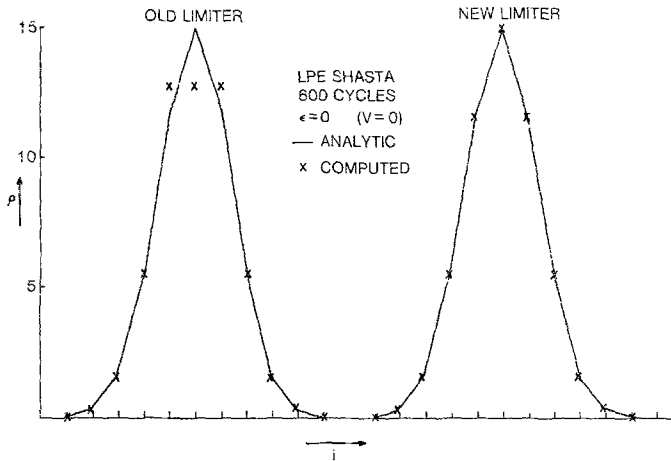

FIG. 4. Comparison of old and new flux limiters on narrow gaussian profile in passive convection for the trivial case of a vanishing velocity field. The transport algorithm is LPE SHASTA. Note the "clipping" phenomenon associated with the old limiter.

case $v = 0$. On the left we see the fimilar "clipping" phenomenon with the original flux limiter, caused by a zeroth order diffusion term in the low order portion of the LPE Shasta algorithm. This diffusion term causes the peak in w^{td} to be smaller than the peak in w_i^n, leaving the original flux limiter (5) with no way of resurrecting the original peak. This process occurs repeatedly, eventually leaving the characteristic three point top. The alternative flux limiter, shown on the right, "remembers" the old value of the peak and is able to resurrect it each time step.

In Fig. 5 we show the same problem after 600 iterations but this time for $\epsilon \equiv v\,\Delta t/\Delta x = 0.1$. We see that clipping occurs with both flux limiters, but to a lesser extent with the alternative flux limiter (6) through (14).

At this point we removed the flux limiter entirely and again ran the problem 600 iterations with $\epsilon = 0.1$. The results convinced us that the amplitude and phase properties of the high order portion of LPE Shasta were incapable of resolving the high wave numbers of which the gaussian is composed. Consequently it was decided
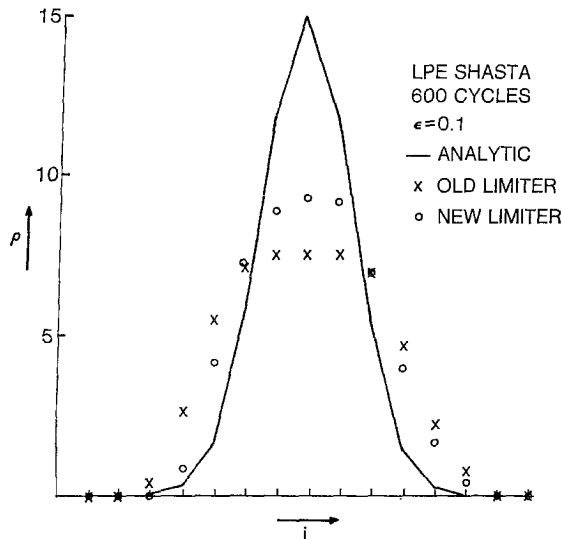
FIG. 5. Same comparison as in Fig. 4 except that the velocity field is now finite. The profile has been convected through 60 grid points. Note the reduced clipping with the new flux limiter.

to switch to a higher order algorithm, a leapfrog-trapezoidal transport algorithm which uses eighth order spatial differences. The algorithm is, then, second order accurate in time and eighth order in space, with an amplification factor that is effectively unity across the entire Fourier spectrum, and phase properties considerably better than those of fourth order algorithms. The leapfrog portion of this algorithm is identical to the eighth order Kreiss–Oliger scheme [6]. A fourth order version of this same algorithm was used later in the two-dimensional solid body rotation tests. We ran the gaussian test problem again 600 iterations with $\epsilon = 0.1$ with *no* flux limiter and were convinced that the algorithm did indeed have the resolving power necessary to do the problem. A low order scheme, donor cell plus a zeroth order diffusion term with coefficient $\frac{1}{8}$, was added to complete the FCT algorithm, which we dub 2–8 leapfrog-trapezoidal. A more detailed description of this algorithm is found in the appendix.

Figure 6 shows the results of 2–8 leapfrog trapezoidal run 600 iterations with $\epsilon = 0.1$ with both the original and alternative flux limiters. The results are better than those in Fig. 5, and again the alternative flux limiter proves superior, but nonthe-
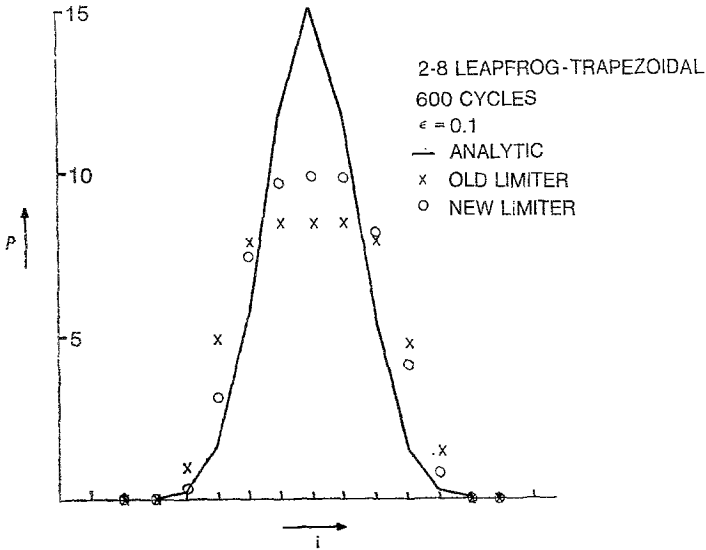
FIG. 6.   Same comparison as in Fig. 5, but with a more accurate transport algorithm (2-8 leapfrog-trapezoidal). Again note the reduced clipping with the new flux limiter.

less disappointing. The clipping would appear to be due entirely to the flux limiters, not to the phase or amplitude properties of the high order scheme.

A careful examination of exactly what happens to a one point peak in a finite difference code reveals the real source of the above problem. Consider a profile
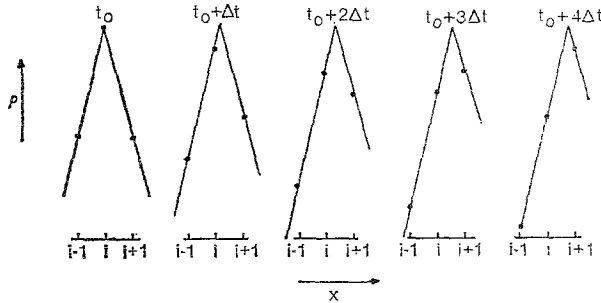

FIG. 7.   Time sequence of profiles produced by a "perfect" convection scheme acting on the variable ρ with $\epsilon = 0.2$. The actual analytic profile is show as a solid line, and the grid point values are shown as dots. Note that at time $t_0 + 4\Delta t$ a grid point value at $(i + 1)$ has been generated which is higher than any grid point value at the previous time step. This is the reason that even the new flux limiter, using Eq. (17) and (18) for w^{max} and w^{min}, must still "clip."

with a local peak at grid point i in passive convection at constant velocity >0. At each succeeding time step the function value at grid point i will decrease and that at $i + 1$ will increase (Fig. 7). Eventually they will both reach some intermediate value, and the actual original peak value will not appear anywhere on the grid, since it's position now lies midway between two grid points. At this point even the

new flux limiter (6) through (14), (17) and (18), has lost the information it needs to allow the peak to be resurrected in suceeding time steps, and will "clip" the new peak at grid point $i + 1$ as it tries to form, based on the assumption that it is, in fact, an overshoot. The effect is magnified, since the clipping itself introduces phase errors in succeeding iterations, the net result being the profiles depicted in Fig. 6.

It is clear, then, that if we are to successfully treat a one-point extremum within the context of FCT we must use information other than just the grid point values themselves. In what follows we shall utilize the flexibility of the alternative flux limiter to use as $w_i^{\max}$ and $w_i^{\min}$ any values that we choose. In Fig. 8 we show a possible way of extracting information about extrema which do not lie exactly on a grid point at the time. Basically we define $w_{i+(1/2)}^{\text{peak}}$ to be the w value at the intersection of the line segments formed by connecting the point (x_{i-1}, w_{i-1}^{td}) with (x_i, w_i^{td}) and the point (x_{i+1}, w_{i+1}^{td}) with (x_{i+2}, w_{i+2}^{td}). If the x coordinate of this intersection lies between x_i and x_{i+1}, then we consider this $w_{i+(1/2)}^{\text{peak}}$ to be an allowable $w^{\max}$ or $w^{\min}$ for either w_i^{n+1} or w_{i+1}^{n+1}. We now have

$$w_i^a = \max(w_i^n, w_i^{td})$$

$$w_i^{\max} = \max(w_{i-1}^a, w_i^a, w_{i+1}^a, w_{i+(1/2)}^{\text{peak}}, w_{i-(1/2)}^{\text{peak}})$$

(19)

$$w_i^b = \min(w_i^n, w_i^{td})$$

$$w_i^{\min} = \min(w_{i-1}^b, w_i^b, w_{i+1}^b, w_{i+(1/2)}^{\text{peak}}, w_{i-(1/2)}^{\text{peak}})$$
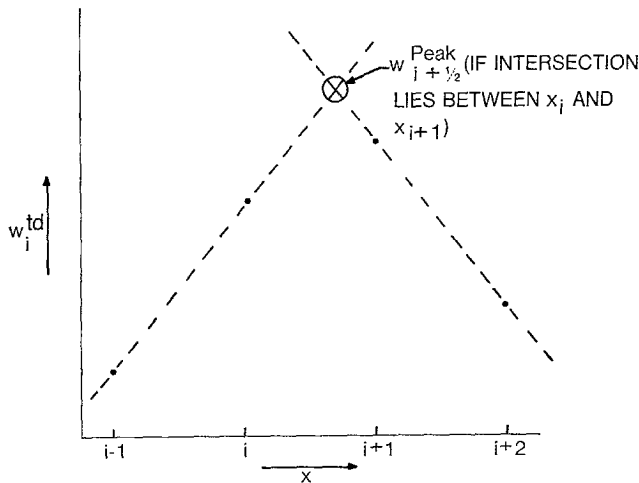
(20)

FIG. 8. A possible scheme for extracting information about extrema which exist *between* grid points at a given point in time. An extremum is assumed to exist between grid points i and $i + 1$ if the intersection of the right and left sided extrapolations of w^{td} has an x coordinate between x_i and x_{i+1}. The w coordinate of the intersection is then used in the computation of $w^{\max}$ and $w^{\min}$ (see text).

Equations (19) and (20) together with Eqs. (6) through (14) now determine the alternative flux limiter (for this section only).

In Fig. 9 we show the results of using Eqs. (19) and (20) to determine w_i^{max} and w_i^{min} on the gaussian test problem run 600 iterations with $\epsilon = 0.1$. Clearly the problem has been solved—we recover the gaussian profile with no dispersive ripples and minimal loss in amplitude. We have not performed this test merely to show the power of the extrapolation technique just described to determine w_i^{max} and w_i^{min}. *Rather this*
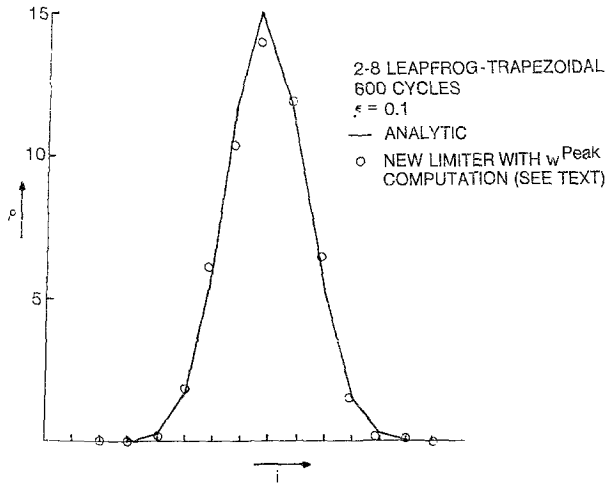
FIG. 9.   Same as Fig. 6, except that Eq. (19) and (20), which utilize the w^{peak} computation illustrated in Fig. 8, are used to compute w^{max} and w^{min} in the new flux limiter. Values for the old flux limiter, since they are identical to those shown in Fig. 6, are not shown. Note that the clipping has been virtually eliminated.

calculation serves to show the power of using information other than that available on the one dimensional grid. In multidimensional flux limiting, this information comes from the other coordinate directions, as we shall see.

VI. FLUX LIMITING IN MULTIDIMENSIONS

The alternative flux limiting algorithm presented in Section IV generalizes trivially to any number of dimensions. For the sake of completeness we present here the algorithm for two spatial dimensions.

Referring to Fig. 10, we seek to limit the antidiffusive fluxes $A_{i+(1/2),j}$ and $A_{i,j+(1/2)}$ such that

$$A^C_{i+(1/2),j} = C_{i+(1/2),j}A_{i+(1/2),j} \qquad 0 \leqslant C_{i+(1/2),j} \leqslant 1$$

$$A^C_{i,j+(1/2)} = C_{i,j+(1/2)}A_{i,j+(1/2)} \qquad 0 \leqslant C_{i,j+(1/2)} \leqslant 1 \tag{6'}$$
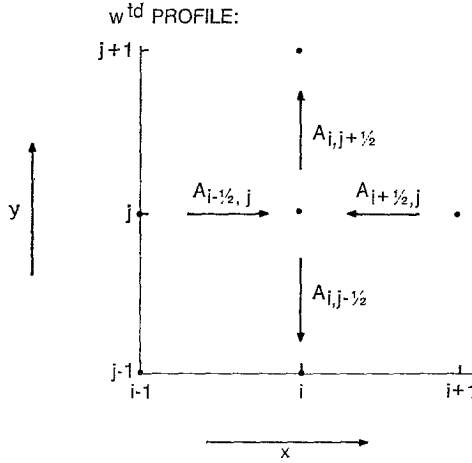
w^{td} PROFILE:

FIG. 10. Two dimensional profile of the transported and diffused values w^{td}, showing the four antidiffusive fluxes $A_{i+(1/2),j}$, $A_{i-(1/2),j}$, $A_{i,j+(1/2)}$, and $A_{i,j-(1/2)}$ whose collective effect must be taken into account with respect to overshoots and undershoots in the final value of $w_{i,j}^{n+1}$. A perspective view of a similar profile is shown in Fig. 2.

and such that $A_{i+(1/2),j}^C$, $A_{i-(1/2),j}^C$, $A_{i,j+(1/2)}^C$, and $A_{i,j-(1/2)}^C$ acting in concert shall not cause

$$w_{i,j}^{n+1} = w_{i,j}^{td} - \Delta V_{i,j}^{-1}[A_{i+(1/2),j}^C - A_{i-(1/2),j}^C + A_{i,j+(1/2)}^C - A_{i,j-(1/2)}^C]$$

to exceed some maximum value $w_{i,j}^{\max}$ nor fall below some minimum value $w_{i,j}^{\min}$.

Again we compute six quantities completely analogous to those computed in Eq. (7) through (12):

$P_{i,j}^+ =$ the sum of all antidiffusive fluxes *into* grid point (i, j)

$$= \max(0, A_{i-(1/2),j}) - \min(0, A_{i+(1/2),j})$$

$$+ \max(0, A_{i,j-(1/2)}) - \min(0, A_{i,j+(1/2)}) \tag{7'}$$

$$Q_{i,j}^+ = (w_{i,j}^{\max} - w_{i,j}^{td}) \Delta V_{i,j} \tag{8'}$$

$$R_{i,j}^+ = \begin{cases} \min(1, Q_{i,j}^+/P_{i,j}^+) & \text{if } P_{i,j}^+ > 0 \\ 0 & \text{if } P_{i,j}^+ = 0 \end{cases} \tag{9'}$$

$P_{i,j}^- =$ the sum of all antidiffusive fluxes *away from* grid point (i, j)

$$= \max(0, A_{i+(1/2),j}) - \min(0, A_{i-(1/2),j})$$

$$+ \max(0, A_{i,j+(1/2)}) - \min(0, A_{i,j-(1/2)}) \tag{10'}$$

$$Q_{i,j}^- = (w_{i,j}^{td} - w_{i,j}^{\min}) \Delta V_{i,j} \tag{11'}$$

$$R_{i,j}^- = \begin{cases} \min(1, Q_{i,j}^-/P_{i,j}^-) & \text{if } P_{i,j}^- > 0 \\ 0 & \text{if } P_{i,j}^- = 0 \end{cases} \tag{12'}$$

Equation (13) becomes

$$C_{i+(1/2),j} = \begin{cases} \min(R^+_{i+1,j}, R^-_{i,j}) & \text{if} \quad A_{i+(1/2),j} \geqslant 0 \\ \min(R^+_{i,j}, R^-_{i+1,j}) & \text{if} \quad A_{i+(1/2),j} < 0 \end{cases}$$

$$C_{i,j+(1/2)} = \begin{cases} \min(R^+_{i,j+1}, R^-_{i,j}) & \text{if} \quad A_{i,j+(1/2)} \geqslant 0 \\ \min(R^+_{i,j}, R^-_{i,j+1}) & \text{if} \quad A_{i,j+(1/2)} < 0 \end{cases} \tag{13'}$$

while Eq. (14) becomes

$$A_{i+(1/2),j} = 0 \quad \text{if} \quad A_{i+(1/2),j}(w^{td}_{i+1,j} - w^{td}_{i,j}) < 0$$

$$\text{and either} \quad A_{i+(1/2),j}(w^{td}_{i+2,j} - w^{td}_{i+1,j}) < 0$$

$$\text{or} \quad A_{i+(1/2),j}(w^{td}_{i,j} - w^{td}_{i-1,j}) < 0 \tag{14'}$$

$$A_{i,j+(1/2)} = 0 \quad \text{if} \quad A_{i,j+(1/2)}(w^{td}_{i,j+1} - w^{td}_{i,j}) < 0$$

$$\text{and either} \quad A_{i,j+(1/2)}(w^{td}_{i,j+2} - w^{td}_{i,j+1}) < 0$$

$$\text{or} \quad A_{i,j+(1/2)}(w^{td}_{i,j} - w^{td}_{i,j-1}) < 0$$

and Eq. (17) and (18) become

$$w^a_{i,j} = \max(w^n_{i,j}, w^{td}_{i,j}) \tag{17'}$$

$$w^{\max}_{i,j} = \max(w^a_{i-1,j}, w^a_{i,j}, w^a_{i+1,j}, w^a_{i,j-1}, w^a_{i,j+1})$$

$$w^b_{i,j} = \min(w^n_{i,j}, w^{td}_{i,j}) \tag{18'}$$

$$w^{\min}_{i,j} = \min(w^b_{i-1,j}, w^b_{i,j}, w^b_{i+1,j}, w^b_{i,j-1}, w^b_{i,j+1})$$

Again, the effect of Eq. (14') is minimal, but if it is used it should be applied *before* Eq. (6') through (13'). Note that our search for $w^{\max}_{i,j}$ and $w^{\min}_{i,j}$ now extends over both coordinate directions. Where finite gradients exist in both directions, this procedure will allow us to stop the clipping phenomenon in regions where a peak exists with respect to one coordinate direction but not in the other, as we shall see in the next section.

Let us comment here on the enforcement of monotonicity in more than one dimension. Equation (6') through (14'), (17') and (18'), and equations of a similar form in three dimensions, will in fact keep the solution within the bounds defined by $w^{\max}$ and $w^{\min}$. This is almost always sufficient to remove the errors due to numerical dispersion ("ripples"). However in more than one dimension this condition is not strictly speaking identical to that of monotonicity enforcement. That is, a solution which was monotonic with respect to one of the coordinate directions, both at the beginning of the time step and in the "transported and diffused" solution w^{td}, might fail to be monotonic with respect to that same coordinate direction at the end of the time step, even though overshoots and undershoots as defined by $w^{\max}$ and $w^{\min}$ were absent. This most often occurs in problems where the quantity of interest

is being transported in a direction perpendicular to a large gradient in that same quantity.

For this reason it is sometimes necessary to impose stronger restrictions on the antidiffusive fluxes. There are several ways to accomplish this, but the simplest is the following:

(1)   For each coordinate direction, limit the antidiffusive fluxes in that direction using Eq. (6) through (14) and either (15) and (16) or (17) and (18). Note that we are not time splitting, since each of the coordinate directions is treated independently and therefore the flux limiting operators commute. If (15) and (16) are chosen, one can equivalently use Eq. (5) for this step.

(2)   Treat the residual corrected fluxes A^C from the above step as if they were the uncorrected fluxes A, and apply the fully multidimensional limiter (6') through (18') or its three dimensional equivalent.

From our limited experience it appears that the above procedure is required only rarely. However, for someone attempting to implement multidimensional FCT for the first time this procedure might be advisable since it is more likely to prevent the occurrence of dispersive ripples under all circumstances. The two dimensional calculations presented in this paper use only Eq. (6') through (14'), (17') and (18').

VII. COMPUTATIONAL EXAMPLES—TWO DIMENSIONS

We choose as our two dimensional test problem that of solid body rotation. That is we have Eq. (3) with $f = w\mathrm{v}_x$, $g = w\mathrm{v}_y$, $\mathrm{v}_x = -\Omega(y - y_0)$, and $\mathrm{v}_y = \Omega(x - x_0)$. Here Ω is the (constant) angular velocity in radians/sec and (x_0, y_0) is the axis of
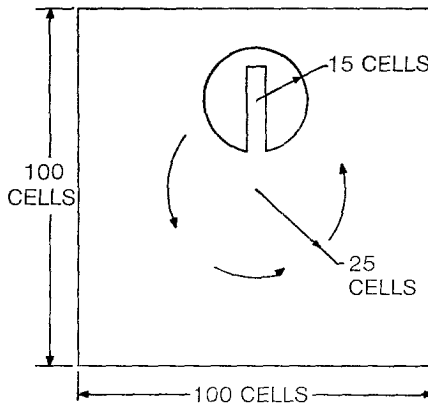

FIG. 11.   Schematic representation of two dimensional solid body rotation problem. Initially w inside the cut-out cylinder is 3.0, while outside $w = 1.0$. The rotational speed is such that one full revolution is effected in 628 cycles. The width of the gap separating the two halves of the cylinder, as well as the maximum extent of the "bridge" connecting the two halves, is 5 cells.
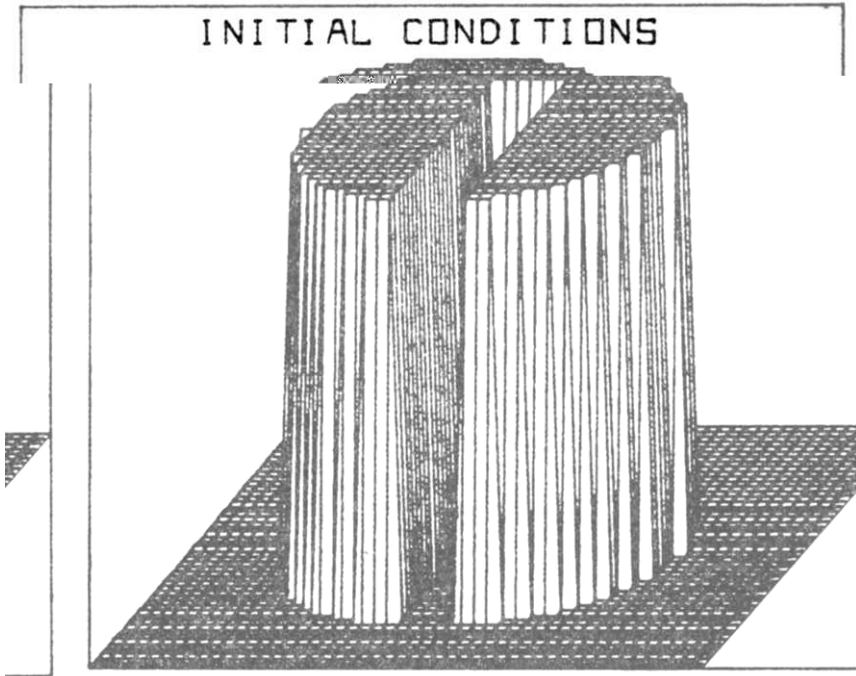
FIG. 12. Perspective view of initial conditions for the two dimensional solid body rotation problem. Note that only a 50 × 50 portion of the mesh centered on the cylinder is displayed. Grid points inside the cylinder have $w_{ij} = 3.0$. All others have $w_{i,j} = 1.0$.

rotation. The configuration is shown in Fig. 11. The computational grid is 100×100 cells, $\Delta x = \Delta y$, with counterclockwise rotation taking place about grid point (50, 50). Centered at grid point (50, 75) is a cylinder of radius 15 grid points, through which a slot has been cut of width 5 grid points. The time step and rotational speed are chosen such that 628 time steps will effect one complete revolution of the cylinder about the central point. A perspective view of the initial conditions is shown in Fig. 12.

Our high order scheme for the following tests is a fully two dimensional, fourth order in space, second order in time leapfrog-trapezoidal scheme, the leapfrog step of which is a two dimensional fourth order Kreiss–Oliger scheme [6]. The low order scheme is simply two dimensional donor cell plus a two dimensional zeroth order diffusion term with diffusion coefficient $\frac{1}{8}$. A more detailed description of this algorithm is found in the appendix.

We wish to emphasize that the *only* difference between calculations in the following comparisons is in the flux limiting stage itself. The high order fluxes, low order fluxes, and hence the (unlimited) antidiffusive fluxes are all computed in the full two dimensions without using time-splitting. In each case we are comparing the fully two dimensional flux limiter given by Eq. (6') through (14'), (17') and (18') with a *time split* application of Eq. (5). Time splitting is the only way that Eq. (5) may be utilized
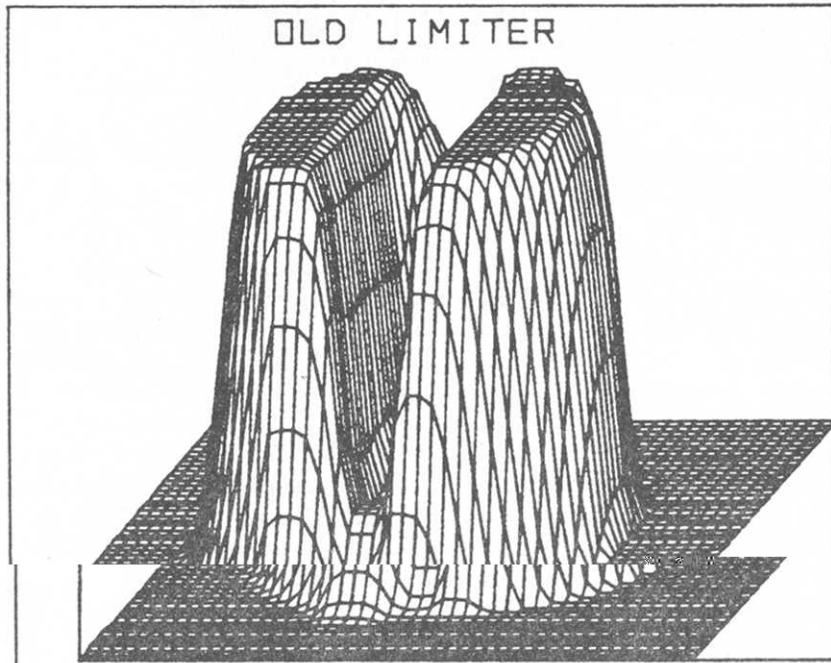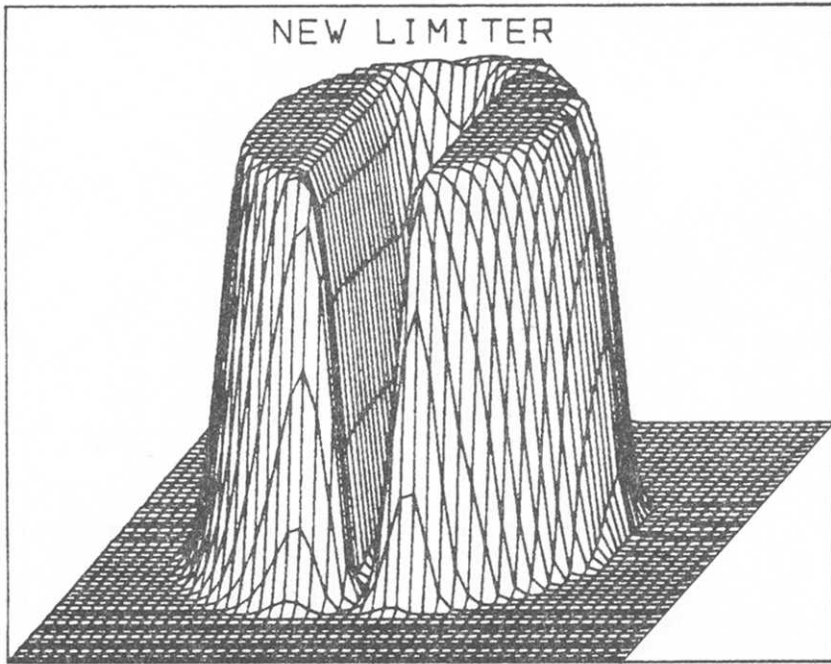
FIG. 13. Comparison of perspective views of the w profile after 157 iterations ($\frac{1}{4}$ revolution) with both the old and new flux limiters. The perspective view has been rotated with the cylinder, so that direct comparison with Fig. 12 can be made. Again we plot only the 50×50 grid centered on the analytic center of the cylinder. Features to compare are the filling-in of the gap, erosion of the "bridge," and the relative sharpness of the profiles defining the front surface of the cylinder.
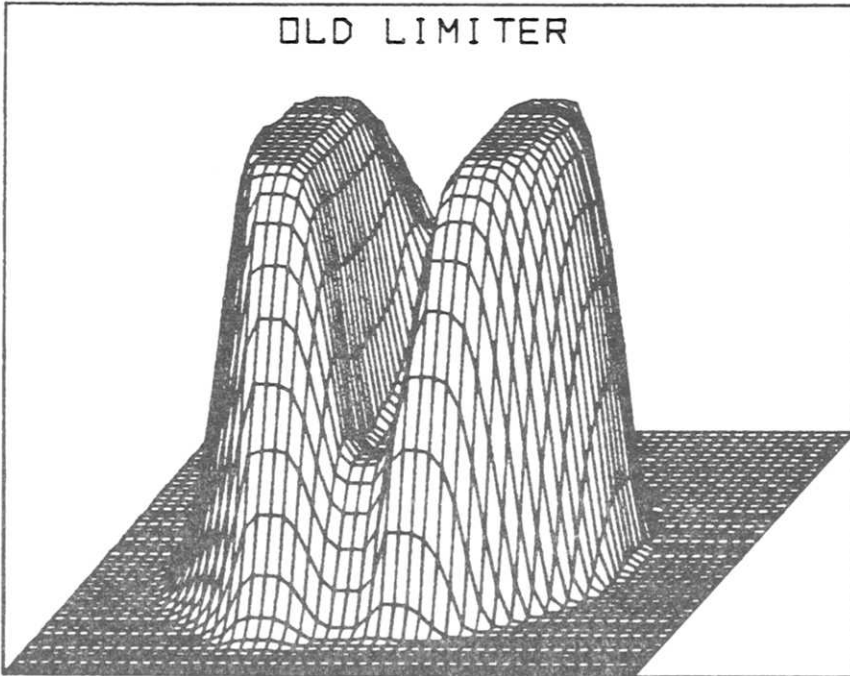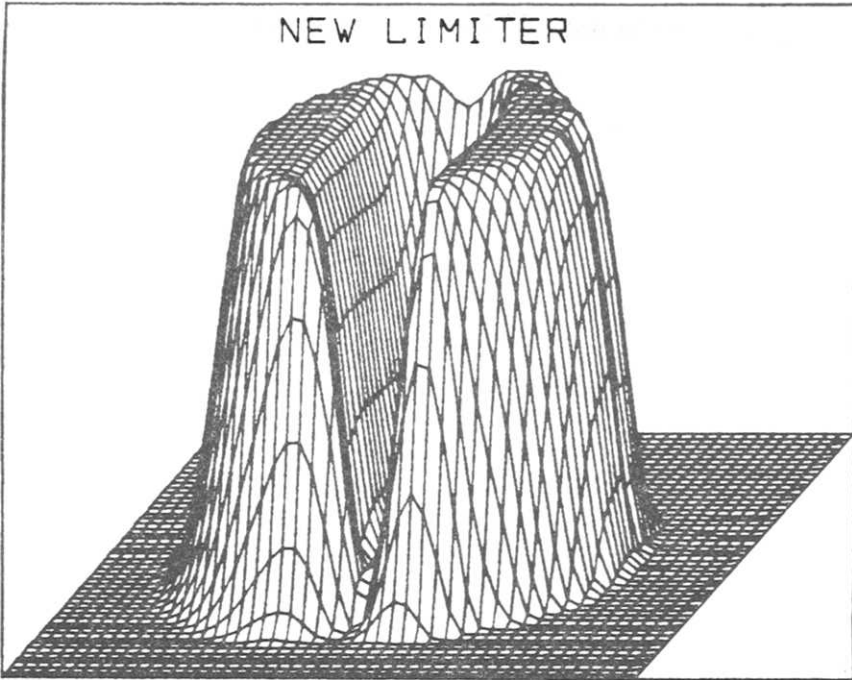
FIG. 14. Same as Fig. 14, but after 628 iterations (one full revolution). Again note decreased diffusion with new flux limiter.

in a multidimensional problem. Note that in the latter case we are *not* time splitting the entire transport operator, but only the flux limiter (5). In this way we are testing only the limiters themselves.

In Fig. 13 we show a perspective view of the two calculations after $\frac{1}{4}$ revolution (157 iterations). Figure 14 presents a comparison of the results of the two calculations for one full revolution (628 cycles). Two features are obvious. The first is a much greater filling-in of the slot with the time split Eq. (5) than with the fully two dimensional flux limiter. The second is the loss of the bridge connecting the two halves of the cylinder in the case of the time-split application of Eq. (5). Less obvious is the *lack of clipping* of the peaked profiles defining the front surface of the cylinder for the case of the fully multidimensional limiter. Clearly this is due to the fact that the multidimensional flux limiter can look in *both* directions to determine whether or not a genuine maximum exists. Note that there are *two* factors working in favor of the fully multidimensional flux limiter: (1) the ability to look in *both* directions to find minima and maxima, as just mentioned; and (2) the ability to scan both w_{ij}^{n} and w_{ij}^{td} to find maxima and minima. Both of these factors are responsible for the improved profiles.

VIII. THE STRIATIONS CODE—A TWO-DIMENSIONAL INCOMPRESSIBLE FLUID CODE USING FULLY MULTIDIMENSIONAL FCT

A two dimensional (x, y) plasma cloud initialized in a region of constant magnetic field $\mathbf{B_0}$ directed along the $\hat{z}$ axis, with an externally imposed electric field $\mathbf{E_0}$ directed along the $\hat{x}$ axis will tend to drift in the $\mathbf{E_0} \times \mathbf{B_0}$ direction (along the negative $\hat{y}$ axis) (see Fig. 15). If the ion-neutral collision frequency is finite, Pedersen conductivity effects will produce polarization fields which tend to shield the inner (more dense) regions of the cloud from $\mathbf{E_0}$, causing this inner portion of the cloud to drift more slowly than the outer portions of the cloud. This results in a steepening of gradients on the *back* side of the cloud. Arguments similar to those above, applied to infinitesimal perturbations imposed upon this back side gradient, show that the back side of the cloud is physically unstable to perturbations along $\hat{x}$. For a detailed description of this problem, see [7].

The equations of motion for the electron fluid are:

$$(\partial N_e / \partial t) + \nabla_{\perp} \cdot (N_e \mathbf{V}_e) = 0 \tag{21}$$

$$\nabla_{\perp} \cdot (N_e \nabla_{\perp} \Psi) = \mathbf{E_0} \cdot \nabla_{\perp} N_e \tag{22}$$

$$\mathbf{V}_e = -(c/B_0) \, \nabla_{\perp} \Psi \times \hat{z} \tag{23}$$

Here N_e, $\mathbf{V}_e$, and Ψ are the electron density, electron velocity and perturbation electric field potential respectively, and $\nabla_{\perp}$ is the two dimensional divergence operator $\hat{x}(\partial/\partial x) + \hat{y}(\partial/\partial y)$. The magnitudes of $\mathbf{B_0}$ and $\mathbf{E_0}$ are 0.5 gauss and 5 millivolts per

meter respectively. Our rest frame here is that of the $(c/B_0) E_0 \times \hat{z}$ velocity. A few trivial vector identities will convince the reader that $\nabla_\perp \cdot V_e = 0$, meaning that the electrons move incompressibly. Clearly time-splitting the transport operator would be disastrous here, and a fully two dimensional scheme is required. In fact, the computational difficulties experienced in trying to solve this problem using time-split applications of one dimensional FCT algorithms were the primary motivating force in the development of the multidimensional flux limiter. The symptoms of the

PLASMA DENSITY
ENHANCEMENT

a) t = 0
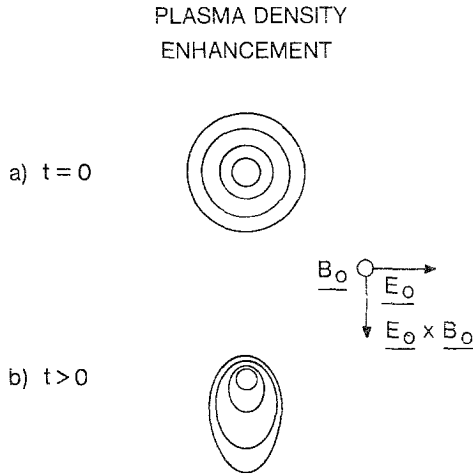
B_0 E_0

$E_0 \times B_0$

b) t > 0

FIG. 15. Schematic representation of the development of a plasma cloud (plasma density increasing toward the center) in crossed electric and magnetic fields. Superimposed on the bulk $E_0 \times B_0$ motion is a steepening of the rearward side of the cloud. This same side is physically unstable to small perturbations.

numerical difficulty were the generation of nonphysical electron densities. This was traced to the false compressibility of the incompressible fluid when seen in each of the splitting directions (consideration of only the x or y components of the electron velocity field yields a non-vanishing divergence).

Equation (22) is solved for Ψ using an elliptic solver, and Eq. (23) then yields the electron velocity field. We then utilize exactly the same multidimensional FCT transport algorithm used in the previous section for solid body rotation to integrate Eq. (21) in time.

Our computational mesh consists of 40 grid points in the $\hat{x}$ direction, 160 grid points in the $\hat{y}$ direction, periodic boundary conditions in both directions, and $\Delta x = \Delta y = 0.31$ km. Our "cloud" consists of a 1-D gaussian:

$$N_e(x, y) = N_0(1 + 10e^{-(y-y_0)^2/64})$$

where N_0 is the ambient background electron density and y_0 is the spatial center of the gaussian distribution. Superimposed upon this distribution is a random x-dependent perturbation with a maximum amplitude of 3 percent.

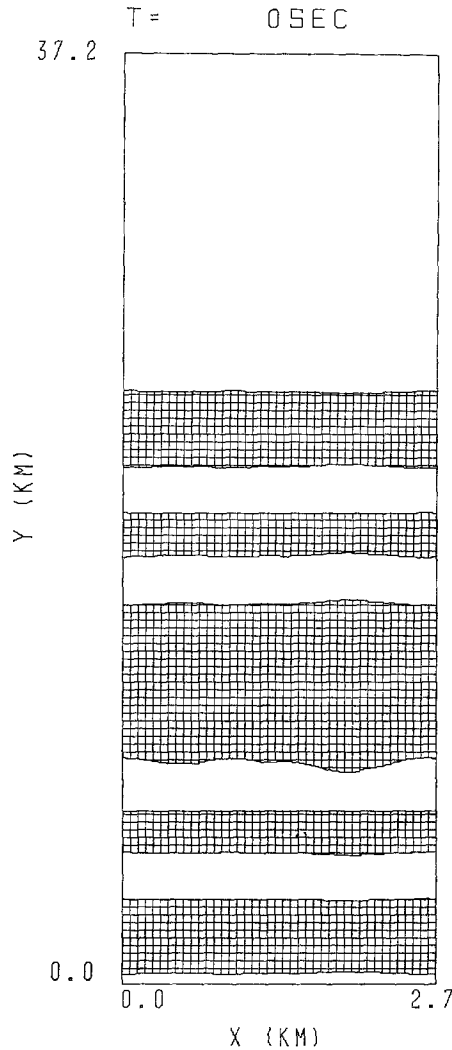Figures 16–20 show isodensity contours of N_e/N_0 for the above configuration at

FIG. 16. Isodensity contours of plasma density at $t = 0$ sec. The initial destribution for N_e/N_0 is a gaussian in y, centered at $y = 12.1$ km, plus a small random perturbation in x. Contours are drawn for $N_e/N_0 = 1.5$, 3.5, 5.5, 7.5 and 9.5. The area between every other contour line is cross-hatched. Only 120 of the 160 cells actually used in the y direction are displayed. Boundary conditions are periodic in both directions. In our plot $\mathbf{B_0}$ is toward the reader, and $\mathbf{E_0}$ is directed toward the right, and we have placed outselves in a frame moving with the $(c/|B_0|^2)\mathbf{E_0} \times \mathbf{B_0}$ velocity. The upper portion of the gaussian is physically unstable to perturbations, while the lower half is (linearly) stable.

various times in the integration. It is seen that, as expected, the back of the cloud (the upper half in the plots) is unstable, growing linearly in the very early stages of development. Non-linear effects soon enter the physics, however, as each striation
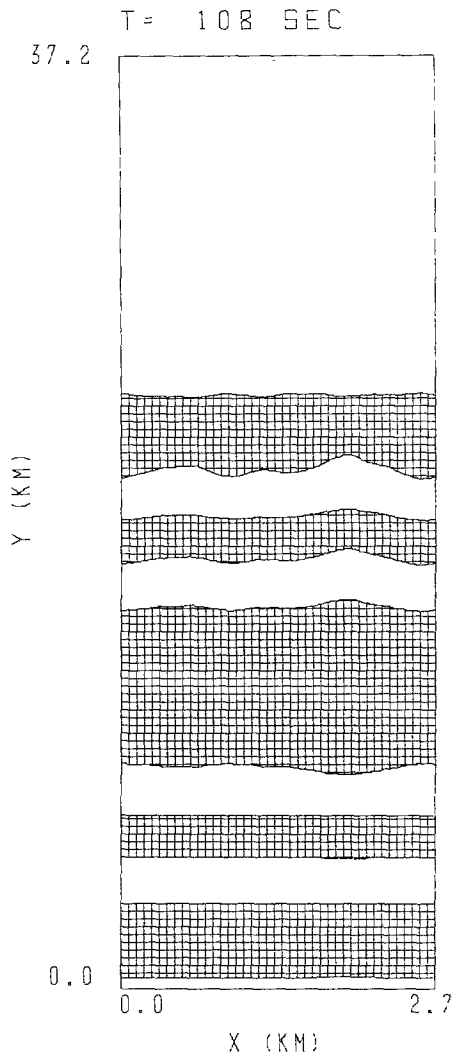
FIG. 17. Same as Fig. 16, but for $t = 108$ sec. Note slow linear growth on unstable side.

successively bifurcates, producing smaller and smaller scale structures, in agreement with the results of the ionospheric barium cloud releases which we are attempting to model. Two points which bear on the numerics should be noted: (1) the intense gradients dictated by the physics are *not* diffused away, nor do there appear in the problem any of the "ripples" associated with numerical dispersion which normally appear when steep gradients try to form; (2) precisely because we did not have to resort to time-splitting, none of the usual time splitting phenomena, such as temporal density oscillations and spurious density values, are evident.
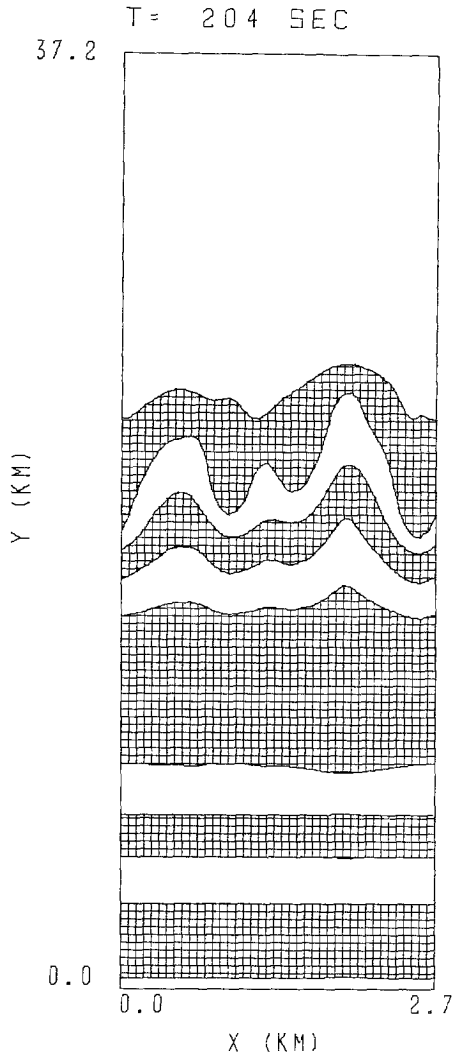
T =   2 0 4   SEC

FIG. 18. Same as Fig. 16, but for $t = 204$ sec. Growth is now much more rapid, and we are entering a highly nonlinear regime.

CONCLUSIONS

We have shown that the algorithm presented in Eq. (6′) through (14′), (17′) and (18′) does, in fact, represent a workable multidimensional flux limiter. In addition, due to the flexibility in determining overshoot and undershoot criteria inherent in the method, the algorithm produces results which are consistently equal or superior to those produced using a time-split version of the original flux limiter (5), at least for the admittedly limited class of problems presented here.
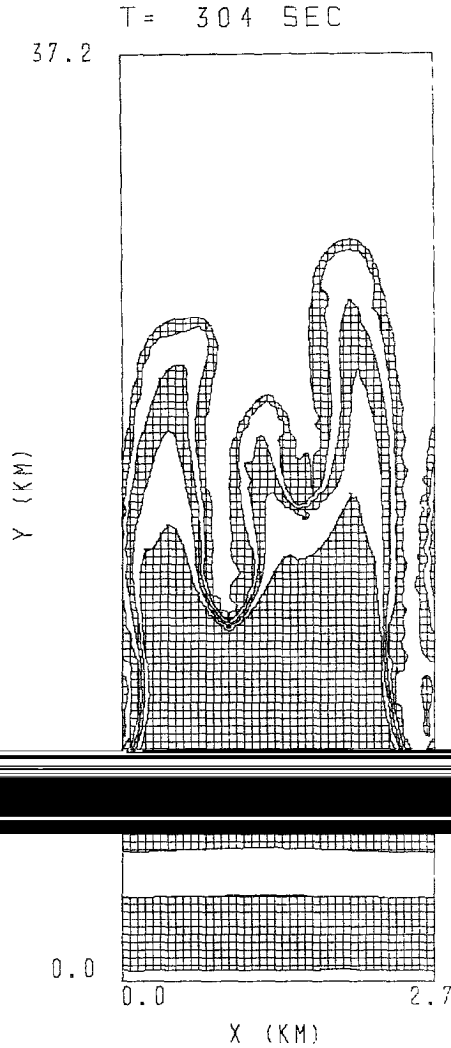
T = 304 SEC

FIG. 19. Same as Fig. 16, but for $t = 304$ sec. Development is fully nonlinear, as the intense gradients and associated high Fourier wave numbers become apparent.

For multidimensional problems where time splitting is unacceptable, or for problems where the "clipping" phenomenon associated with the original flux limiter (5) is a serious problem, the new algorithm presented here represents the only way that FCT may be implemented. For these problems the choice is clear, for there is only one option. Yet even in situations where the constraints mentioned above do not apply, benefit may be gained by implementing the new algorithm rather than time splitting Eq. (5). We do not yet have enough experience to give any guidelines, and can only ask the prospective user to try the method.
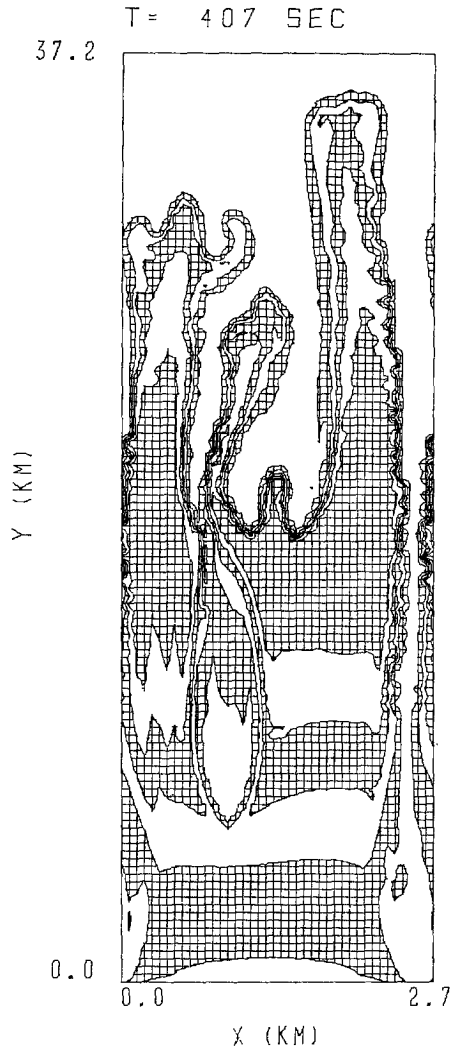
FIG. 20. Same as Fig. 16, but for $t = 407$ sec. Several plasma bifurcations are apparent, in agreement with the experimental results from ionospheric barium cloud releases, and we have maximum to minimum density variations resolved over only 2 cells.

Certainly the possibilities for modifying the basic scheme are endless. One could, for instance, limit the antidiffusive fluxes only with respect to maxima, or to minima; or he could limit the fluxes *sequentially* for maxima and minima, rather than limiting maxima and minima simultaneously in the manner presented here (this last procedure will introduce an asymmetry between the treatment of maxima and minima which may or may not be desirable). Even within time-split codes there are possibilities. One could time split the one dimensional form of the new algorithm rather

than time splitting Eq. (5); or fully multidimensional flux limiting could be performed at the end of each sweep of a time-split scheme.

On NRL's Texas Instruments ASC computer, the calculations presented in Section VII required 93 seconds and 125 seconds of CPU time for the time-split and fully multidimensional cases respectively, a cost penalty of slightly more than 30 % for the multidimensional limiter. The Fortran coding was entirely vectorized in both calculations. Of course this extra cost is highly problem dependent. For instance the striations code described in Section VIII spends 80 % of its time solving Eq. (22), making the net cost penalty of fully multidimensional flux limiting only a few percent.

APPENDIX: BRIEF DESCRIPTION OF LEAPFROG-TRAPEZOIDAL TRANSPORT ALGORITHMS

We seek finite difference approximations to the equation

$$w_t + f_x = 0 \tag{A1}$$

We assume that at the beginning of a time step, values of w_i and f_i are known at grid points x_i and at time levels $t - \Delta t$ and t. The leapfrog-trapezoidal finite difference approximation to Eq. (A1) in flux form is:

$$w_i' = w_i^{t-\Delta t} - 2 \Delta t \, \Delta x_i^{-1} [F_{i+(1/2)}^t - F_{i-(1/2)}^t] \tag{A2}$$

$$f_i^* = \tfrac{1}{2}(f_i^t + f_i') \tag{A3}$$

$$w_i^{t+\Delta t} = w_i^{\ t} - \Delta t \, \Delta x_i^{-1}(F_{i+(1/2)}^* - F_{i-(1/2)}^*) \tag{A4}$$

Here $F^t \equiv F(f^t)$ and $F^* \equiv F(f^*)$. Note that here our fluxes $F_{i+(1/2)}$ differ from those described in the text by factors of $2\Delta t$ and Δt in Eq. (A2) and (A4) respectively.

The trapezoidal step Eq. (A3) and (A4) strongly damps the computational mode generated in the leapfrog step Eq. (A2). Time centering in both steps guarantees second order accuracy in time. The trapezoidal step was implemented at each iteration for the calculations presented in Section VII, and at every fourth iteration for those presented in Sections V and VIII.

If Δx_i is independent of i, the following difference forms give the indicated order of spatial accuracy:

Second order:

$$F_{i+(1/2)} = \tfrac{1}{2}(f_{i+1} + f_i)$$

Fourth order:

$$F_{i+(1/2)} = \tfrac{7}{12}(f_{i+1} + f_i) - \tfrac{1}{12}(f_{i+2} + f_{i-1})$$

Sixth order:

$$F_{i+(1/2)} = \tfrac{37}{60}(f_{i+1} + f_i) - \tfrac{2}{15}(f_{i+2} + f_{i-1}) + \tfrac{1}{60}(f_{i+3} + f_{i-2})$$

Eighth order:

$$F_{i+(1/2)} = \tfrac{533}{840}(f_{i+1} + f_i) - \tfrac{139}{840}(f_{i+2} + f_{i-1}) + \tfrac{29}{840}(f_{i+3} + f_{i-2}) - \tfrac{1}{280}(f_{i+4} + f_{i-3})$$

The above fourth and eighth order forms are used as the high order fluxes in the main body of this paper.

The low order flux of the leapfrog-trapezoidal FCT schemes is simply donor cell plus a zeroth order diffusive flux with coefficient $\tfrac{1}{8}$. The donor cell algorithm requires, that $f = vw$, where v is a convective velocity. Specifically,

$$F^L_{i+(1/2)} = v_{i+(1/2)} w^{DC}_{i+(1/2)} - \tfrac{1}{8}(x_{i+1} - x_i)(w^0_{i+1} - w_i{}^0) \, \Delta t^{-1}$$

where

$$v_{i+(1/2)} \equiv \tfrac{1}{2}(v_i + v_{i+1})$$

$$w^{DC}_{i+(1/2)} = \begin{cases} w_i{}^0 & \text{if } v_{i+(1/2)} \geqslant 0 \\ w_{i+1}{}^0 & \text{if } v_{i+(1/2)} < 0 \end{cases}$$

$$w_i{}^0 = \begin{cases} w_i{}^{n-1} & \text{for leapfrog step} \\ w_i{}^n & \text{for trapezoidal step} \end{cases}$$

A detailed description and analysis of these and other high order FCT algorithms will be discussed in a forthcoming report by the present author.

ACKNOWLEDGMENTS

REFERENCES

1. J. P. BORIS AND D. L. BOOK, *J. Comput. Phys.* **11** (1973), 38.
2. D. L. BOOK, J. P. BORIS, AND K. HAIN, *J. Comput. Phys.* **18** (1975), 248.
3. J. P. BORIS AND D. L. BOOK, *J. Comput. Phys.* **20** (1976), 397.
4. D. GOTTLIEB, *SIAM J. Numer. Anal.* **9** (1972), 650.
5. C. K. FORESTER, *J. Comput. Phys.* **23** (1977), 1.
6. H.-O. KREISS AND J. OLIGER, *Tellus* **24** (1972), 199.
7. A. J. SCANNAPIECO, S. L. OSSAKOW, S. R. GOLDMAN, AND J. M. PIERRE, *J. Geophys. Res.* **81** (1976), 6037.
8. A. HARTEN AND G. ZWAS, *J. Comput. Phys.* **9** (1972), 568.